

WANG, Y., WANG, S., FAN, Y., XIE, Y. and FERNANDEZ, C. 2022. A novel adaptive back propagation neural network-unscented Kalman filtering algorithm for accurate lithium-ion battery state of charge estimation. *Metals* [online], 12(8), article 1369. Available from: <https://doi.org/10.3390/met12081369>

# A novel adaptive back propagation neural network-unscented Kalman filtering algorithm for accurate lithium-ion battery state of charge estimation.



WANG, Y., WANG, S., FAN, Y., XIE, Y. and FERNANDEZ, C.

2022

© 2022 by the authors. Licensee MDPI, Basel, Switzerland. This article is an open access article distributed under the terms and conditions of the Creative Commons Attribution (CC BY) license (<https://creativecommons.org/licenses/by/4.0/>).

## Article

# A Novel Adaptive Back Propagation Neural Network-Unscented Kalman Filtering Algorithm for Accurate Lithium-Ion Battery State of Charge Estimation

Yangtao Wang <sup>1</sup>, Shunli Wang <sup>1,2,\*</sup> , Yongcun Fan <sup>1</sup>, Yanxin Xie <sup>1</sup> and Carlos Fernandez <sup>3</sup> <sup>1</sup> School of Information Engineering, Southwest University of Science and Technology, Mianyang 621010, China<sup>2</sup> College of Electrical Engineering, Sichuan University, Chengdu 610065, China<sup>3</sup> School of Pharmacy and Life Sciences, Robert Gordon University, Aberdeen AB10-7GJ, UK

\* Correspondence: wangshunli@swust.edu.cn

**Abstract:** Accurate State of Charge (SOC) estimation for lithium-ion batteries has great significance with respect to the correct decision-making and safety control. In this research, an improved second-order-polarization equivalent circuit (SO-PEC) modelling method is proposed. In the process of estimating the SOC, a joint estimation algorithm, the Adaptive Back Propagation Neural Network and Unscented Kalman Filtering algorithm (ABP-UKF), is proposed. It combines the advantages of the robust learning rate in the Back Propagation (BP) neural network and the linearization error reduction in the Unscented Kalman Filtering (UKF) algorithm. In the BP neural network part, the self-adjustment of the learning factor accompanies the whole estimation process, and the improvement of the self-adjustment algorithm corrects the shortcomings of the UKF algorithm. In the verification part, the model is validated using a segmented double-exponential fit. Using the Ampere-hour integration method as the reference value, the estimation results of the UKF algorithm and the Back Propagation Neural Network and Unscented Kalman Filtering (BP-UKF) algorithm are compared, and the estimation accuracy of the proposed method is improved by 1.29% under the Hybrid Pulse Power Characterization (HPPC) working conditions, 1.28% under the Beijing Bus Dynamic Stress Test (BBDST) working conditions, and 2.24% under the Dynamic Stress Test (DST) working conditions. The proposed ABP-UKF algorithm has good results in estimating the SOC of lithium-ion batteries and will play an important role in the high-precision energy management process.

**Keywords:** lithium-ion battery; equivalent model; state of charge; iterative calculation; ABP-UKF algorithm



**Citation:** Wang, Y.; Wang, S.; Fan, Y.; Xie, Y.; Fernandez, C. A Novel Adaptive Back Propagation Neural Network-Unscented Kalman Filtering Algorithm for Accurate Lithium-Ion Battery State of Charge Estimation. *Metals* **2022**, *12*, 1369. <https://doi.org/10.3390/met12081369>

Academic Editor: Yoshikazu Ito

Received: 11 June 2022

Accepted: 15 August 2022

Published: 18 August 2022

**Publisher's Note:** MDPI stays neutral with regard to jurisdictional claims in published maps and institutional affiliations.



**Copyright:** © 2022 by the authors. Licensee MDPI, Basel, Switzerland. This article is an open access article distributed under the terms and conditions of the Creative Commons Attribution (CC BY) license (<https://creativecommons.org/licenses/by/4.0/>).

## 1. Introduction

With the continuous shifting of the national energy structure, the development of new energy has also shown unprecedented opportunities, and lithium-ion batteries have been widely used and developed. Since the 1990s, the lithium-ion battery industry has played an irreplaceable role in the global energy storage market [1]. Lithium electrification, energy savings, and high speed will be the future of the industry. To achieve this goal, accurate SOC estimation is of great significance, giving full play to the performance [2,3], real-time monitoring, and safety control of lithium-ion batteries [4]. At the same time, lithium-ion battery recycling has also been widely studied [5,6], which has the effect of protecting the environment and will create huge economic benefits. Recycling mainly consists of battery destruction to extract metal raw materials and cascade utilization. To determine which application is to be carried out, accurate estimation of the SOC of lithium-ion batteries is a prerequisite.

The estimation of the SOC depends on an equivalent model that relies on the cell battery characteristics, that is the internal activity of the cell [7,8]. However, due to the complex working conditions and the complex internal structure of lithium-ion batteries [9–11], the

battery often exhibits drastic nonlinear characteristics [12–14]. Based on this, a new model needs to be developed to replace the traditional one to describe the operating characteristics of lithium-ion batteries [15,16]. Currently, the commonly used battery models include equivalent circuit models [17], electrochemical models [18,19], and thermal coupling models [20–22]. Among the various methods of modelling lithium-ion batteries, the equivalent circuit model is the most widely used method, and both the electrochemical model and the thermal coupling model take into account the knowledge of chemistry and physics, which affects the estimation of the complex operating conditions at a later stage.

The algorithms used to estimate the SOC include the open-circuit voltage method, the Ampere-hour (Ah) integration method, the Kalman filter algorithm [23], and the neural network algorithm [24,25]. Due to the complex working conditions and the complex electrochemical reaction inside the battery, the ohmic effect, the self-discharge effect, etc., the results of the traditional state of charge estimation have a large error [26,27]. Therefore, researchers have proposed an improved algorithm based on the traditional one [28–30]; there are also data-driven methods for estimating the state of charge of lithium-ion batteries [31–34], and some of the proposed algorithms by the latter are effective in state of charge estimation. Regarding the current status of the literature, a simple equivalent model is easy to calculate, but cannot accurately describe the operating characteristics of the battery [35,36]; however, a complex equivalent model can better characterize the charging and discharging characteristics of the batteries, but the computational effort will increase significantly, reducing the applicability of the model [37]. Considering these factors, an SO-PEC model for lithium-ion batteries has been established. Compared with the Thevenin model [38], the complexity of the SO-PEC model is moderate. The internal polarization reaction of the battery is divided into two parts: rapid reaction and slow reaction, and the two groups of polarization circuits represent these, respectively. The four parameters that can be obtained are used as the input values of the BP neural network, and the correction compensation value obtained through network training is particularly effective for SOC compensation. Therefore, the proposed SO-PEC model can better characterize the internal chemical reaction of lithium-ion batteries.

As a nonlinear system estimation method, the UKF algorithm abandons the idea of the approximate linearization of nonlinear functions, which undoubtedly has certain advantages over the Kalman algorithm to a certain extent. However, in the later stage of SOC estimation, the filtering error will be larger than the average level, and it easily deviates from the reference value. Therefore, considering the robust learning of the neural network algorithm for data processing, an appropriate BP neural network algorithm is selected for the error compensation of the UKF algorithm [39]. The problem of how to adjust the connection weights of the hidden layer has long existed in the study of neural network algorithms until the introduction of the BP neural network, which successfully solved the problem of weight adjustment for multi-layer feed-forward neural networks with nonlinear functions. The BP neural network is a multi-layer feed-forward network trained according to the error back propagation algorithm, and the input layer of the BP neural network is used to receive information from the outside world and pass it on to the hidden layer; the hidden layer is the information processing layer, responsible for the conversion of the internal information; the information passed from the hidden layer to the output layer is further processed to complete the neural network learning process.

Although the BP neural network has a strong self-learning ability when dealing with large-scale data, the obtained network performance is poor, and the learning rate is unstable. In this study, algorithmic adjustment of the adaptive learning rate can make up for the problem of the estimated value deviating from the mean value when estimating the SOC by the UKF algorithm and meet the conditions for optimizing the BP neural network. To sum up, based on the UKF algorithm, given the error in the SOC estimation process, the ABP is proposed to correct the error of the UKF algorithm to estimate the SOC. In the results verification part, the data under domestic and foreign working conditions are simulated

and analysed, and the Ampere-hour integration, UKF algorithm, and BP-UKF algorithm are compared.

In this research, the second section is the mathematical analysis, and it has four parts: the analysis of the SO-PEC model, segmental parameter identification, the ABP-UKF algorithm, and the SOC estimation model. The third section is the analysis of the experimental verification; this section first introduces the experimental platform and, then, gives a complete description of the analysis of the model verification and estimation result; the former obtains data under HPPC working conditions, and the latter conducts experimental verification under three working conditions: HPPC, BBDST, and DST. After a complete closed-loop logic, the ABP-UKF algorithm proposed in this research shows good results in estimating the SOC of lithium-ion batteries.

## 2. Mathematical Analysis

### 2.1. The SO-PEC Modelling Method

The premise of accurately estimating the SOC is to establish an accurate battery model. The most commonly used model is the Thevenin model, but a single Resistance-Capacitance (RC) parallel circuit cannot accurately characterize the dynamic characteristics of lithium-ion batteries; therefore, the SO-PEC modelling method is proposed. Compared with the Thevenin equivalent circuit model, an RC parallel circuit is added, which better simulates the existence of the internal polarization effect of the battery, and the model does not become complicated. The model consists of static ohmic resistance  $R_0$  in series with two RC parallel circuits, which characterize the dynamic response. The SO-PEC model can simulate the dynamic and static characteristics of the lithium-ion batteries well, and the complexity is moderate, making it easy to implement in engineering. The state of charge estimation of the lithium-ion battery can be implemented based on the parameters of the equivalent circuit. The SO-PEC model is shown in Figure 1.

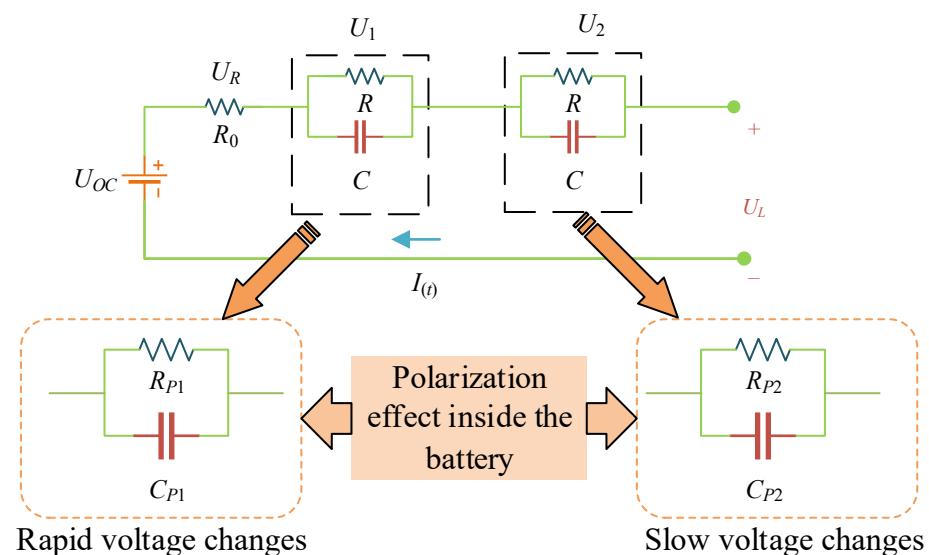


Figure 1. The SO-PEC model.

In Figure 1,  $U_{OC}$  represents the open-circuit voltage,  $U_L$  represents the terminal voltage,  $R_0$  is the ohmic resistance, and the voltage drop across  $R_0$  is  $U_L$ . In order to characterize the polarization effect of the lithium-ion battery, RC parallel circuits are composed of a polarization resistance  $R_P$  and a polarization capacitance  $C_P$ , where  $R_{P1}$  and  $C_{P1}$  represent the phase of rapid voltage change during the chemical reaction inside the battery, and the RC circuit consisting of  $R_{P2}$  and  $C_{P2}$  represents the phase of slow voltage change during the chemical reaction inside the battery. According to Kirchhoff's law, the voltage and current

expressions of the equivalent circuit can be obtained by analysing the model, as shown in Equation (1).

$$\begin{cases} U_L = U_{oc} - U_R - U_{p1} - U_{p2} \\ I(t) = C_{p1} \frac{dU_1}{dt} + \frac{U_1}{R_{p1}} = C_{p2} \frac{dU_2}{dt} + \frac{U_2}{R_{p2}} \end{cases} \quad (1)$$

The  $SOC_0$  is the initial SOC value, and the equation for calculating the SOC can be obtained by combining the definition of the SOC, as shown in Equation (2).

$$SOC_k = SOC_0 - \frac{\eta \int_0^k i(t) dt}{Q_0} \quad (2)$$

In Equation (2),  $\eta$  is the discharge efficiency of the lithium-ion battery, which is generally taken as  $\eta = 1$  at room temperature.  $Q_0$  is the rated capacity of the batteries. The setting of the initial value of  $SOC_0$  is based on the following: when experimenting with a full-capacity lithium-ion battery,  $SOC_0 = 1$ , it should be mentioned that: if you want to test the tracking of an algorithm of the real-time state of the system, you can set an inaccurate initial value to verify the tracking performance of the algorithm.

For Equations (1) and (2), the open-circuit voltage  $U_{OC}$  can be represented by the state variable SOC, selecting  $x_k = [SOC_k, U_{p1,k}, U_{p2,k}]^T$  as the state space variable; the input variable is  $i_k$ ; the output variable is  $y_k = [U_{L,k}]$ . The state space equations are discretized to obtain the equation shown in Equation (3).

$$\begin{cases} x_{k+1} = \begin{bmatrix} 1 & 0 & 0 \\ 0 & e^{-\frac{\Delta t}{\tau_1}} & 0 \\ 0 & 0 & e^{-\frac{\Delta t}{\tau_2}} \end{bmatrix} x_k + \begin{bmatrix} -\frac{\Delta t}{Q_0} \\ R_1(1 - e^{-\frac{\Delta t}{\tau_1}}) \\ R_2(1 - e^{-\frac{\Delta t}{\tau_2}}) \end{bmatrix} i_k + w_k \\ y_k = U_{oc,k} - R_0 i_k + [0 \quad -1 \quad -1] x_k + v_k \end{cases} \quad (3)$$

In the above equation,  $\Delta t$  is the sampling time interval,  $\tau_1 = R_{p1}C_{p1}$ ,  $\tau_2 = R_{p2}C_{p2}$ ,  $w$  is the system noise,  $v$  is the measurement error noise, and  $w$  and  $v$  are Gaussian white noise.  $Q_0$  is the rated capacity of the battery. The parameters  $R_0$ ,  $U_{OC}$ ,  $R_{p1}$ ,  $R_{p2}$ ,  $C_{p1}$ , and  $C_{p2}$  can be obtained by the HPPC working conditions, and the mathematical relationship obtained by the above state-space equation can characterize the working characteristics of lithium-ion batteries. This research used CFTOOL in MATLAB to perform the curve fitting of the data to obtain the identification parameters.

## 2.2. Segmented Double-Exponential Fit Parameter Identification

Ternary lithium-ion batteries were selected for the research, while the nominal capacity of the batteries is 45 Ah and the actual capacity is 43.68 Ah. To obtain the variations of the external parameters to characterize the operating characteristics of the Li-ion battery, HPPC tests were carried out on the Li-ion battery at 25 °C. Comprehensive consideration and online parameter identification can improve the estimation accuracy of the SOC to a certain extent; this will increase the complexity of the algorithm, while the improvement effect is not visible. Therefore, the segmented double-exponential fit method was put forward for parameter identification. The segmented double-exponential fitting selects the zero-state response of the charge-discharge stage at the point of 10 SOC portions and simulates the entire experiment with 100 data per group, for a total of 1000 data. The battery was subjected to HPPC working conditions at 25 °C. The sampling experiment was set to 0.1 s. The voltages and currents during the charging and discharging for the whole HPPC experiment are shown in Figure 2.

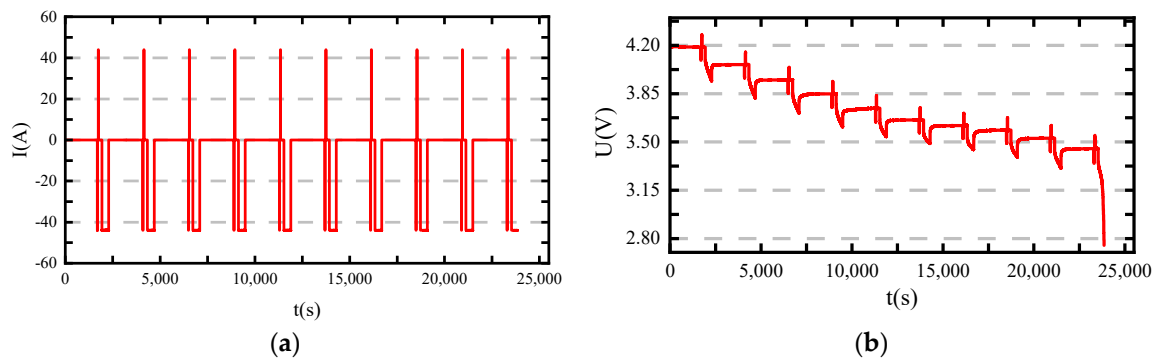


**Figure 2.** The voltage and current curve of the whole HPPC process. (a) The current curve of the HPPC process. (b) The voltage curve of the HPPC process.

Figure 2 shows the HPPC experiment that was carried out at points with an SOC of 1.0, 0.9, 0.8, . . . , 0.2, 0.1, and the charge and discharge rates were set at 1C, while the steps of the single cycle were constant current discharge pulses, a 40 s rest, 10 s constant current charge pulses, and pulse cycles half an hour apart at the neighbouring SOC points.

Figure 3 shows the change process of the charge and discharge voltage when SOC = 0.9. Analysing the data of the discharge process: The  $U_{OC}$  is the stable voltage at the positive and negative ends of the battery when the battery is shelved for a long time. In this experiment, the voltage of the lithium-ion battery is stable after shelving for 30 min, and the voltage value at this time can be equivalent to the open-circuit voltage value. When SOC = 0.9,  $U_1$  can be taken as the open-circuit voltage value. The open-circuit voltage data can be read out directly from the data obtained from the HPPC working conditions.

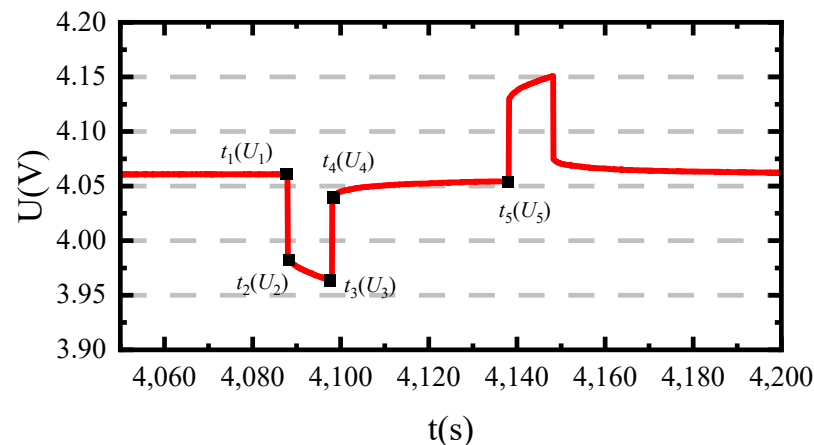


**Figure 3.** Voltage curve at SOC = 0.9.

In the two time periods of  $t_1 \sim t_2$  and  $t_3 \sim t_4$ , the voltage change is mainly affected by the ohmic resistance of the battery. The calculation expression of the ohmic resistance can be obtained as shown in Equation (4).

$$R_0 = \frac{(U_1 - U_2) + (U_4 - U_3)}{2I} \tag{4}$$

During the period from  $t_2$  to  $t_3$ , the terminal voltage of the lithium-ion battery slowly drops from  $U_2$  to  $U_3$ , which is the zero-state response. Performing time-domain analysis on this zero-state response circuit, a functional relationship between  $U_L$  and time  $t$  can be obtained, as shown in Equation (5).

$$U_L(t) = U_{OC} - IR_{p1} \left(1 - e^{-t/\tau_1}\right) - IR_{p2} \left(1 - e^{-t/\tau_2}\right) \tag{5}$$

Equation (5) can be written as a multi-parameter unknown functional relationship, as shown in Equation (6).

$$\begin{cases} y = a^{-\frac{x}{c}} + b^{-\frac{x}{d}} + e \\ R_{p1} = \frac{a}{I}, R_{p2} = \frac{b}{I} \\ C_{p1} = \frac{c}{R_{p1}}, C_{p2} = \frac{d}{R_{p2}} \end{cases} \quad (6)$$

Using 10 pulses of discharge data under the HPPC working conditions, the parameters described can be determined by fitting the equation using Equation (6) as the target equation. In Equation (6), five parameters, a, b, c, d, and e, can be obtained, as well as the relationship between them, and the parameters required in this research are also expressed in it, where e is the value of  $U_{OC}$ ; the required parameters can be obtained after calculation.

### 2.3. Adaptive BP Neural Network-Unscented Kalman Algorithm

In the current research of lithium-ion batteries, researchers often combine equivalent circuits with adaptive algorithms such as Kalman filters for battery SOC estimation. However, for the nonlinear problem of the state of charge estimation of lithium-ion batteries, researchers often use the extended Kalman filter and unscented Kalman filter or data-driven methods to deal with this problem. The EKF algorithm expands the nonlinear function with Taylor series and turns the nonlinear system into a linear system. However, the EKF method can only retain the first-order derivative term and constant term of the nonlinear function, ignore its higher-order derivative terms, and estimate the battery's SOC with a large error. The UKF method uses Unscented Transformation (UT) to process the data, uses UT transformation to expand the data length, weights and reconstructs the original data, keeps the mean and variance of the data unchanged, and uses the expanded data to transform the nonlinear system. Compared with the EKF method, the parameter estimation error is smaller. Therefore, this study used the UKF estimation results as the benchmark to explore the related algorithms. Here, the BP neural network with the simplest structure was selected as the neural network algorithm to correct the UKF estimation results.

The key to the UKF algorithm is the traceless transformation problem. The fundamental principle is to obtain a certain number of sampling points according to a fixed sampling method (usually symmetric sampling) based on the statistical properties of the state variables, which need to have the same mean and covariance as the original state variables. The above point set is nonlinearly transferred using the state equation, and the transformed mean and covariance can be obtained according to the weight distribution. Throughout the process, the sampling points can be obtained as shown in Equation (7).

$$\begin{cases} x^i = \hat{x}, i = 0 \\ x^i = \hat{x} + \left(\sqrt{(n+\lambda)P}\right)_i, i = 1 \sim n \\ x^i = \hat{x} - \left(\sqrt{(n+\lambda)P}\right)_{i-n}, i = n+1 \sim 2n \end{cases} \quad (7)$$

The dimension of the state variable  $x$  is  $n$ ;  $\hat{x}$  and  $P$  are their mean and covariance matrix, respectively; the corresponding weights are shown in Equation (8).

$$\begin{cases} \omega_m^0 = \frac{\lambda}{n+\lambda} \\ \omega_c^0 = \frac{\lambda}{n+\lambda} + (1 - \alpha^2 + \beta) \\ \omega_m^i = \frac{\lambda}{2(n+\lambda)}, i = 1 \sim 2n \\ \omega_c^i = \frac{\lambda}{2(n+\lambda)}, i = 1 \sim 2n \end{cases} \quad (8)$$

where  $\omega$  are the corresponding weights,  $\alpha$ ,  $\beta$ , and  $\lambda$  are scaling parameters (usually, the value rule is that:  $\beta \geq 0$ , normally = 2,  $0.2 \leq \alpha \leq 1$ ,  $\lambda = \alpha^2(n+\kappa) - n$ ,  $\kappa$  is the auxiliary scale factor, and  $\kappa = 3 - n$ ). In this research, the central idea of the adaptive BP neural network algorithm used to correct for the error is to make the value of the learning rate a variable that selects the learning factor, and the learning rate is defined as Equation (9).

$$\mu(k+1) = \begin{cases} k_a \mu(n) & E(k+1) < E(k) \\ k_b \mu(n) & E(k+1) > E(k) \end{cases} \quad (9)$$



In Equation (9),  $\mu$  is the learning rate,  $k_a$  is the learning rate increment factor,  $k_b$  is the learning rate decrement factor, and  $E$  is the error value. Combined with the above correlation analysis, the ABP–UKF algorithm is obtained to estimate the state of charge of lithium-ion batteries. After receiving the external voltage and current data, the data are entered into the UKF algorithm for iteration, then the input values required for the BP neural network are obtained, then sent to the adaptive neural network for training, and the trained data are used as a correction value to complete the whole process of iteration and estimation.

The algorithm implementation of ABP-UKF is divided into three stages: prediction, update, and correction of the error, which refers to the final processing of the data. The flowchart is shown in Figure 4.

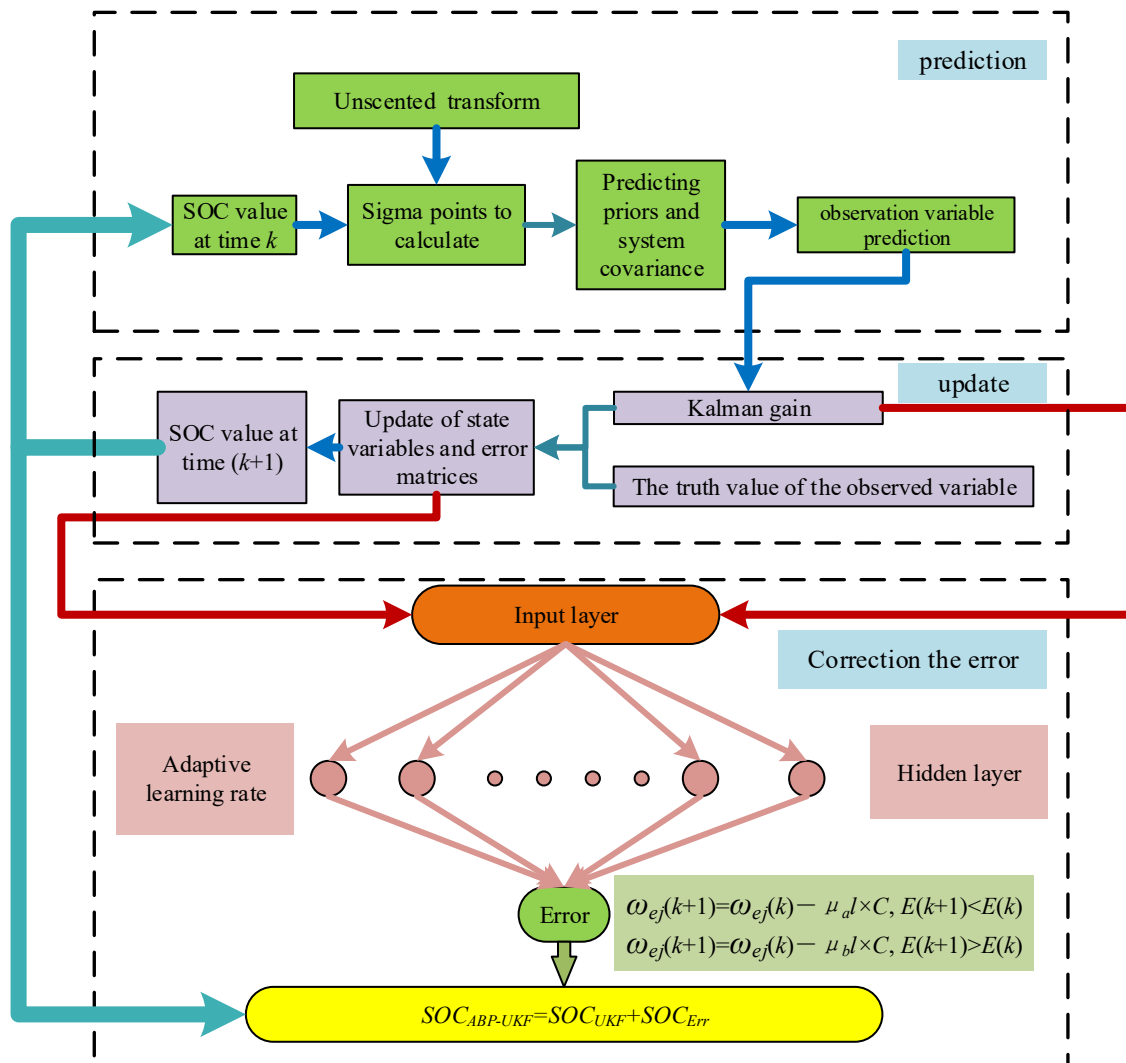


Figure 4. Block diagram of the ABP-UKF algorithm.

Through the sampling of unscented transformation sampling points and the acquisition of the corresponding weights, coupled with the characteristics of the automatic adjustment of the learning rate of the BP neural network, the logical analysis of the SOC estimation algorithm is carried out according to Figure 4, divided into three parts as follows:

1. Prediction stage:



Predict the system state variables and the error variance matrix at time  $k+1$ ; combined with Equation (8), the weighted sum is obtained to obtain the predicted mean value of the system state quantity, which can be calculated as shown in Equation (10).

$$\left\{ \begin{array}{l} \hat{x}_{k+1|k} = \sum_{i=0}^{2n} \omega_m^i x_{k+1|k}^i \\ P_{xx,k+1|k} = \sum_{i=0}^{2n} \omega_c^i [x_{k+1|k}^i - \hat{x}_{k+1|k}] [x_{k+1|k}^i - \hat{x}_{k+1|k}]^T + Q_{k+1} \end{array} \right. \quad (10)$$

where  $i = 1, 2, 3, \dots, 2n + 1$  (unscented transform of all points).  $x$  is the state variable.  $w$  is the corresponding weights.  $P_{xx}$  is the error variance matrix.  $Q$  is the Gaussian noise. Then, update the weight of the average of the measured values and the variance matrix of the measurement at time  $k + 1$ , and finally, obtain the variance matrices of the state and measurement quantities at  $k + 1$ .

$$\left\{ \begin{array}{l} \hat{y}_{k+1|k} = \sum_{i=0}^{2n} \omega_m^i y_{k+1|k}^i \\ P_{yy,k+1} = \sum_{i=0}^{2n} \omega_c^i [y_{k+1|k}^i - \hat{y}_{k+1|k}] [y_{k+1|k}^i - \hat{y}_{k+1|k}]^T + R_{k+1} \\ P_{xy,k+1} = \sum_{i=0}^{2n} \omega_c^i [x_{k+1|k}^i - \hat{x}_{k+1|k}] [y_{k+1|k}^i - \hat{y}_{k+1|k}]^T \end{array} \right. \quad (11)$$

where  $y$  is the predicted value of each sampling point (it is a map of  $x$ ) and  $x_k$  is the input variable.  $P_{yy}$  is the variance matrix of the measurement.  $P_{xy}$  is the variance matrices of state and measurement value.  $R$  is the noise at this time.

## 2. Update stage:

Kalman filter gain:

$$K_{k+1} = \frac{P_{xy,k+1}}{P_{yy,k+1}} \quad (12)$$

Update the system state variable values and error variance matrix.

$$\left\{ \begin{array}{l} \hat{x}_{k+1|k+1} = \hat{x}_{k+1|k+1} + K_{k+1} (y_{k+1} - \hat{y}_{k+1|k}) \\ P_{xx,k+1|k+1} = P_{xx,k+1|k} - K_{k+1} P_{xy,k+1} K_{k+1}^T \end{array} \right. \quad (13)$$

## 3. Error correction stage:

The entire neural network is divided into two processes: forward transmission and reverse transmission of the error signals. First, the Kalman filter gain matrix  $K_{k+1}$  and the state of charge estimation matrix error  $P_{xx}$  obtained from the training dataset in the UKF algorithm are used as the input layer of the BP neural network. During the forward propagation process, each node output value is  $a_j$ , and this  $a_j$  is based on the output values of all nodes in the upper layer, the weights of the current node and all nodes in the previous layer, the threshold of the current node, and the activation function. The specific calculation is shown in Equation (14).

$$\left\{ \begin{array}{l} S_j = \sum_{e=0}^{m-1} \omega_{ej} a_e + b_j \\ a_j + f(S_j) = \frac{1 - e^{-S_j}}{1 + e^{-S_j}} \end{array} \right. \quad (14)$$

The weight between node  $e$  and node  $j$  is  $\omega_{ej}$ ; the threshold of node  $j$  is  $b_j$ ;  $f(S_j)$  is the activation function. In this study, the sigmoid function was used to output after processing. In the process of BP, the weights and thresholds are repeatedly corrected, so that the target output error is optimized in the required direction. For the error function in the neural

network and according to the gradient descent method, the gradient value for the  $j$ th node is shown in Equation (15).

$$\begin{cases} E(\omega, b) = \frac{1}{2} \sum_{j=0}^{n-1} (d_j - y_j)^2 \\ \frac{\partial E(\omega, b)}{\partial \omega_{ej}} = (d_j - y_j) f(S_j) \cdot (1 - f(S_j)) \end{cases} \quad (15)$$

The result of the output layer is  $d_j$ .  $y_j$  is the error correction value of the UKF algorithm, and we obtain the weight between the hidden layer and the output layer as follows.

$$\omega_{ej} = \omega_{ej} - l \cdot \frac{\partial E(\omega, b)}{\partial \omega_{ej}} \quad (16)$$

In the above equation,  $l$  is the learning rate. This research improved the learning rate so that it can choose the learning factor according to the correction process and can be optimized according to Equation (17) to update the weights.

$$\begin{cases} \omega_{ej}(k+1) = \omega_{ej}(k) - \mu_a l \cdot \frac{\partial E(\omega, b)}{\partial \omega_{ej}}, E(k+1) < E(k) \\ \omega_{ej}(k+1) = \omega_{ej}(k) - \mu_b l \cdot \frac{\partial E(\omega, b)}{\partial \omega_{ej}}, E(k+1) > E(k) \end{cases} \quad (17)$$

After completing this part of the data processing, the error correction value of the UKF algorithm is obtained, and finally, the final estimation calculation of the SOC is performed, as shown in Equation (18).

$$SOC_{ABP-UKF} = SOC_{UKF} + SOC_{Err} \quad (18)$$

$SOC_{ABP-UKF}$  is the estimated value obtained;  $SOC_{UKF}$  is the estimated value of the UKF algorithm;  $SOC_{Err}$  is the error value obtained by the neural network after training, also called the correction value.

When the ABP-UKF algorithm estimates the SOC of the lithium-ion battery, the target estimator SOC is used as the state variable, and the battery terminal voltage is the observed variable. It can be seen from the results that in the later estimation process, the compensation effect of the ABP algorithm on the UKF algorithm has a visible optimization effect in the final estimation result. The validity of the algorithm proposed in this research is verified again.

#### 2.4. SOC Estimation Model

Combined with the descriptions in Sections 2.2 and 2.3, the SOC estimation model for lithium-ion batteries can be established, and the model flow is shown in Figure 5. It consists of three main parts: model validation, network training, and SOC estimation; the latter two parts as a whole, estimating the SOC of lithium-ion batteries, require two sets of data, which are used as the training dataset and the test dataset for the relevant iterative calculations.

As shown in Figure 5, the entire SOC estimation model is divided into three parts: accurate lithium-ion battery modelling is the premise of accurately estimating the SOC; the SO-PEC model used in this study can well characterize the working conditions of lithium-ion batteries; training the network is the key to SOC estimation; in this research, by using the ABP-UKF algorithm and the relevant training of the estimation results of the UKF algorithm, the estimation error of the algorithm will be corrected, which improves the estimation efficiency to a certain extent; the final SOC estimation is the verification of the proposed algorithm, and the three parts are indispensable. Through this figure, it can be seen that the iteration of data and the algorithm process are the overall logical framework of this research.

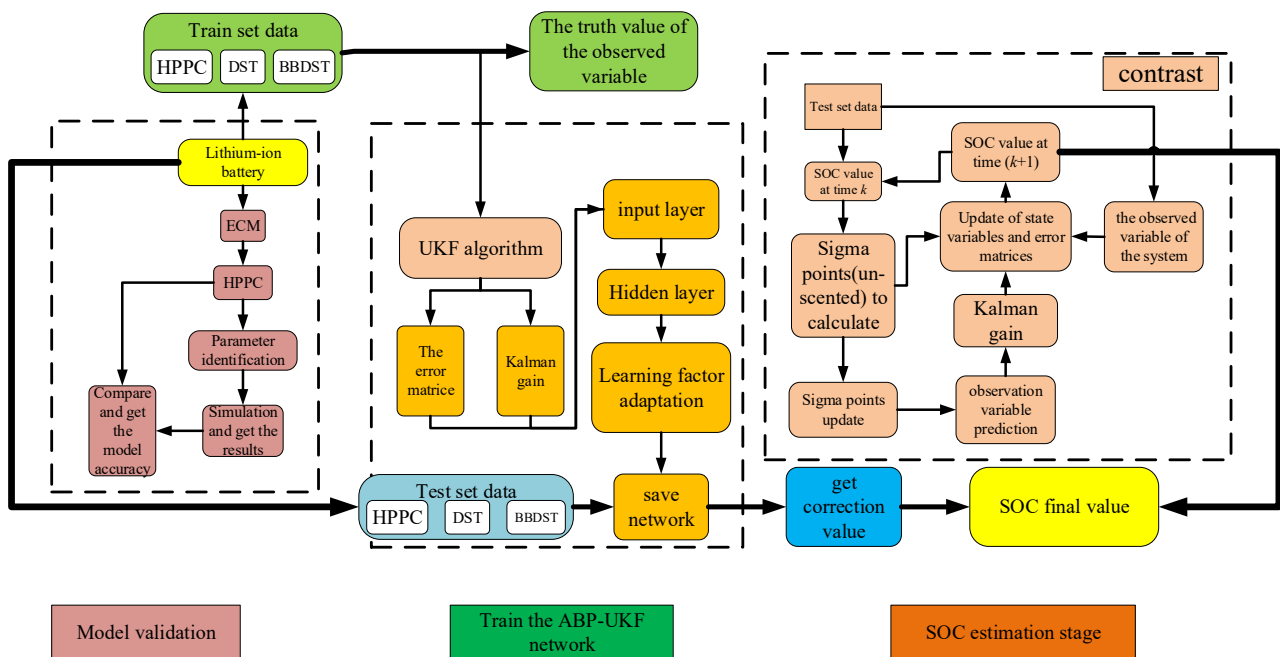


Figure 5. Lithium-ion battery state of charge estimation model.

### 3. Experimental Analysis

#### 3.1. Experimental Platform

All three experiments, HPPC, BBDST, and DST, were carried out on the experimental platform. The experimental platform is shown in Figure 6.

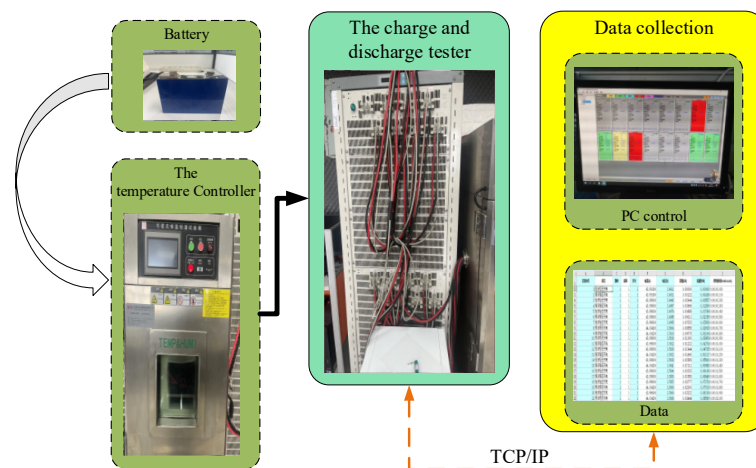


Figure 6. Experimental platform.

As shown in Figure 6, all experiments were conducted with a lithium-ion battery with a rated capacity of 45 Ah as the subject of study, which was placed in a temperature controller to reduce the influence of temperature on the working conditions of the lithium-ion battery and the charge and discharge experiments under various working conditions. On the PC side, set the working conditions, perform simulated charging and discharging, obtain experimental data such as voltage, current, capacity, and temperature, then process the data, select the data segment, and conduct relevant verification.

### 3.2. Model Validation

The HPPC working conditions were performed on the 10 divided points. Between the point states of the SOC, enough time is needed to make the battery return to normal, without polarization reaction, electrochemistry, and thermal equilibrium, so we set a 30 min shelf time. The required polarization resistance and polarization capacitance values are shown in Table 1.

**Table 1.** Results of the model parameters.

SOC (100%)	$U_{OC}$ (V)	$R_{P1}$ ( $\Omega$ )	$R_{P2}$ ( $\Omega$ )	$C_{P1}$ (F)	$C_{P2}$ (F)	$R_0$ ( $\Omega$ )
1.0	4.1908	0.000813409	0.000118136	19,867.00196	4740.284725	0.003418182
0.9	4.0662	0.000790455	0.000124977	17,825.18689	4750.463721	0.003452273
0.8	3.9574	0.000835455	0.000123182	17,104.46137	5072.98893	0.003465909
0.7	3.8581	0.000958864	0.000116818	17,593.74259	7138.44358	0.003486364
0.6	3.7434	0.000933182	0.000121909	17,177.7886	5753.467562	0.003479545
0.5	3.6718	0.000768636	$9.17727 \times 10^{-5}$	25,512.71437	12814.26449	0.003515909
0.4	3.6321	0.000685455	$9.08409 \times 10^{-5}$	23,896.55172	7258.844133	0.003536364
0.3	3.5946	0.000596364	$8.62955 \times 10^{-5}$	20,356.70732	4685.067158	0.003579545
0.2	3.5388	0.000995909	$9.25455 \times 10^{-5}$	23,214.97033	9668.762279	0.003643182
0.1	3.4712	0.000972955	0.00011625	15,447.79257	5238.709677	0.003738636

The data shown in Table 1 were fed into the simulation software, where the equivalent circuit model was simulated to obtain the accuracy of the model estimation of the SO-PEC modelling method. The model, which can accurately characterize the operating state of a lithium-ion battery, is a prerequisite for the accurate estimation of the lithium-ion battery's state of charge. The comparison and error figure of the simulated SO-PEC voltage and the reference data are shown in Figure 7.

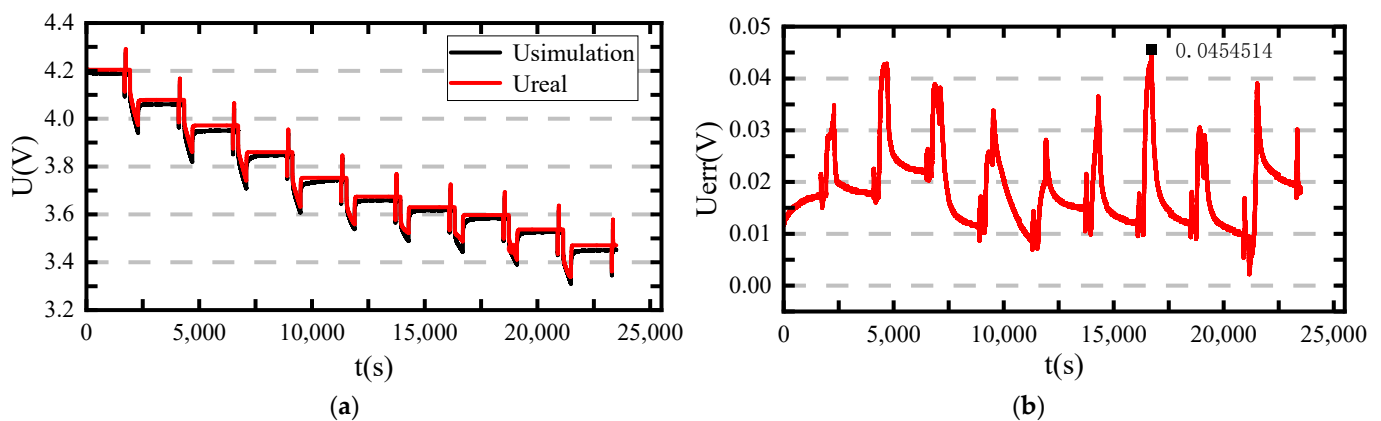


**Figure 7.** Model validation results comparison and error. (a) Comparison of model validation results. (b) Error of model validation results.

From the data analysis in Figure 7, it can be seen that in the simulation process of the model, the maximum error value is 0.0455 V, and the accuracy of the model estimation according to Equation (19) reaches 98.915%. Accurate model simulation is the premise of accurately estimating the SOC of lithium-ion batteries, so the SO-PEC in this research can well characterize the working conditions of lithium-ion batteries.

$$E_{s,err} = \frac{U_{rr}}{U_{oc,1}} \quad (19)$$

$E_{s,err}$  is the estimation accuracy;  $U_{rr}$  is the value of the estimation error;  $U_{oc,1}$  is the open-circuit voltage when the SOC is 1.

### 3.3. Analysis of the SOC Estimated Results in Complex Working Conditions

After the model validation in Section 3.2, the model used in this paper to characterize the operating state of the Li-ion battery is shown to be sufficiently accurate. Next, the estimation results of the model and algorithm proposed in this paper needed to be validated under various working conditions. To verify whether the algorithm proposed in this research can be optimized for the deviation of the estimated difference of the UKF algorithm from the mean value under different working conditions, the model was mainly verified under HPPC working conditions, BBDST working conditions, and DST working conditions.

#### 3.3.1. Analysis of the Results under HPPC Working Conditions

Lithium-ion batteries are discharged intermittently in daily use, and with this feature in mind, the algorithm model can be verified under HPPC working conditions. The SOC estimation results and errors under HPPC working conditions are shown in Figure 8.

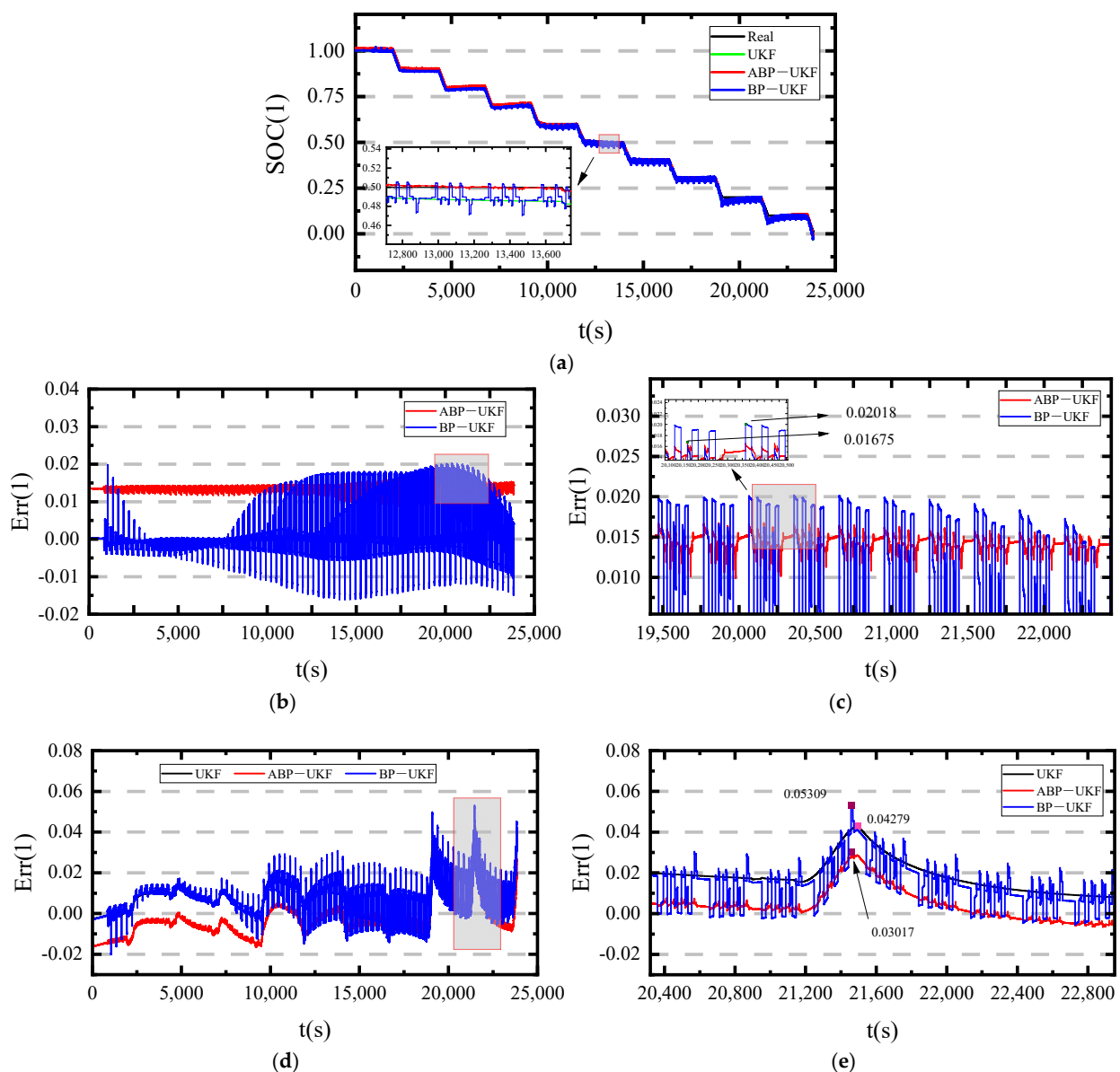


**Figure 8.** SOC estimation and error comparison under HPPC. (a) Estimation results of the SOC under the HPPC working conditions. (b) Correction value based on the UKF algorithm. (c) Enlarged view of the correction value based on the UKF algorithm. (d) Error of the SOC under the HPPC working conditions. (e) Enlarged view of the error of the SOC under the HPPC working conditions.

Figure 8a is the SOC estimation results of various algorithms under the HPPC experimental conditions; Figure 8b is the correction value of the BP-UKF and the ABP-UKF based on the UKF estimation results; Figure 8c is the partially enlarged view of Figure 8b; Figure 8d is based on the SOC value estimated by the reference value, the error curve of the UKF, the BP-UKF, the ABP-UKF algorithms, respectively; Figure 8e is the partially enlarged diagram of Figure 8c. It can be seen from Figure 8a that the overall SOC estimation effect of the UKF algorithm and the BP-UKF algorithm fluctuates greatly, and the proposed ABP-UKF algorithm can track the SOC well in the entire estimation process with slight fluctuations; the estimation result of the ABP-UKF algorithm can be closer to the reference value. The UKF algorithm and the BP-UKF algorithm have local oscillations, which can partly explain why the proposed algorithm can effectively correct the error estimated by the UKF algorithm, and the proposed algorithm has better performance on the tracking performance. From the corrected error curve in Figure 8b, the convergence of the ABP-UKF algorithm is better than that of the BP-UKF algorithm, and the enlarged curve can also reveal this result more clearly. The error curve of Figure 8d shows that the maximum error estimated by the UKF algorithm is 4.31%. Because of the oscillation of the estimated results of the BP-UKF algorithm, the maximum error reaches 5.31%. The BP algorithm can correct the estimated value of UKF to a certain extent, but it will generally oscillate within a certain range. The maximum estimated error of the ABP-UKF algorithm is 3.02%, which can greatly attenuate the compensatory oscillation of the BP-UKF algorithm. The modification of the ABP algorithm to the UKF algorithm was verified, and the estimation results were modified and optimized. The criteria for the SOC estimation results under the HPPC working conditions are shown in Table 2.

**Table 2.** Criteria for the SOC estimation results under HPPC working conditions.

Reference Value	Algorithm	MAX	MAE	RMSE
Ah	UKF	0.04309	0.01005	0.01248
	BP-UKF	0.05309	0.00916	0.00013
	ABP-UKF	0.03017	0.00702	0.00007
UKF	BP <sub>cor</sub>	0.02018	0.00405	0.00005
	ABP <sub>cor</sub>	0.01675	0.01381	0.00019

In Table 2, the metrics of the SOC estimates obtained using the Ah-integral method as the reference value and the algorithm correction result measurement obtained by the UKF algorithm estimate as the reference value are shown, respectively. BP<sub>cor</sub> represents the compensation value of the BP algorithm on the UKF algorithm. The UKF algorithm is directly compensated by the compensation value obtained by network training with the error and Kalman gain as the input. ABP<sub>cor</sub> represents the compensation value of the ABP algorithm on the UKF algorithm. MAX is the maximum value, and the MAE can better reflect the actual situation of the error of the predicted value. The RMSE measures the deviation between observations and reference values. The ABP-UKF algorithm has the smallest estimation error, and it had the best performance regarding the MAE and RMSE among the three algorithms. From Figure 8b,c and the correction values: the correction effect of the ABP algorithm on the initial value is evident, although the correction value of the ABP-UKF algorithm is less than the correction value of the BP algorithm, and the BP algorithm had better performance regarding the MAE and RMSE, while the ABP algorithm has a more evident correction effect on the overall compensation; it can obtain better performance results.

### 3.3.2. Analysis of Results under BBDST Working Conditions

In actual operation, the charging and discharging process of the battery is complex, with instantaneous high current shock and rapid switching of the charging–discharging process, placing extremely high demands on the performance of the battery. This operating

condition is a work-step simulation of the actual operation of an electric bus in Beijing. The dynamic test condition BBDST was used for experimental verification [40]. The SOC estimation results verified by operating conditions are shown in Figure 9.

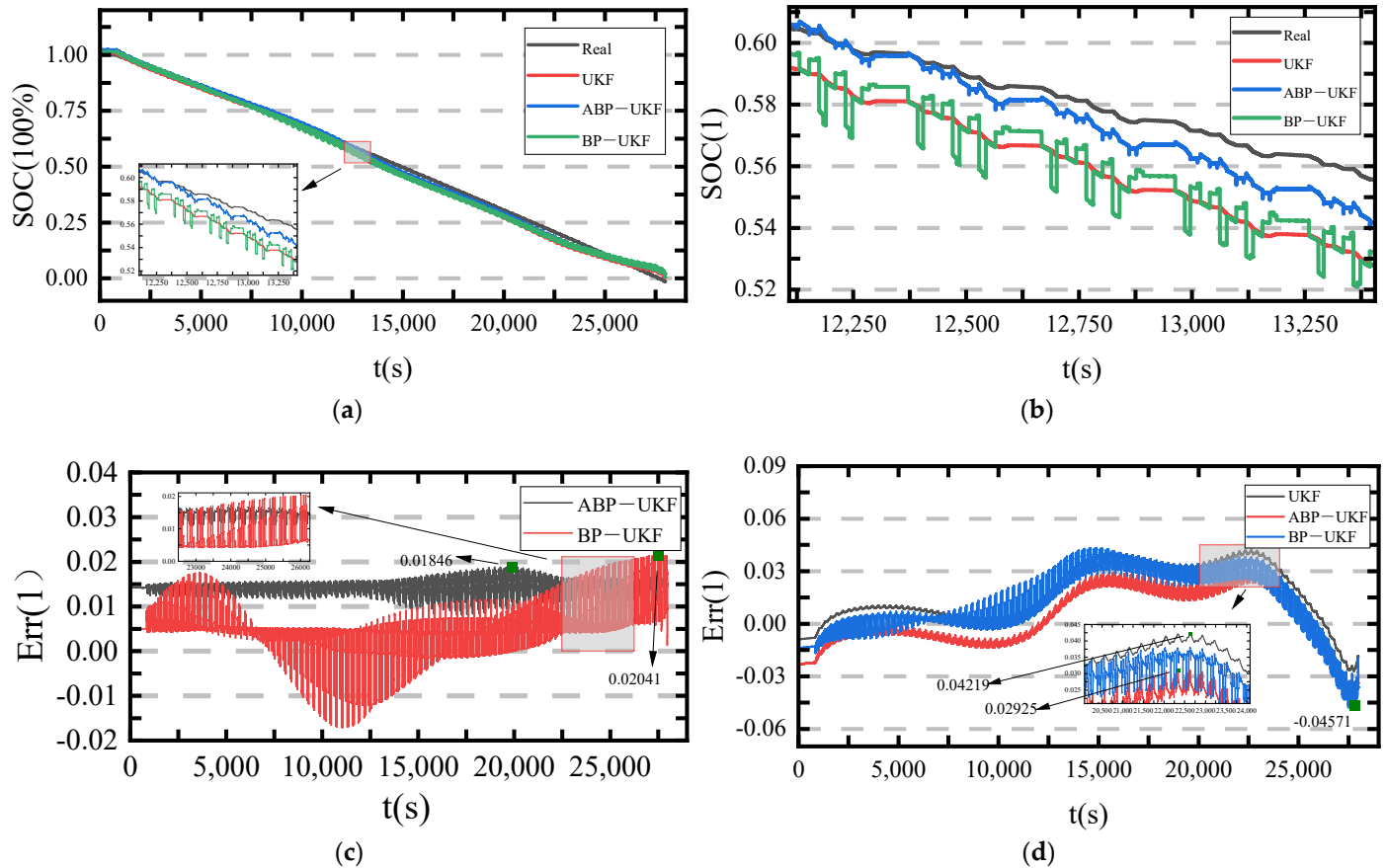


**Figure 9.** SOC estimation and error comparison under BBDST. (a) Estimation results of the SOC under the BBDST working conditions. (b) Enlarged view of the estimation results of the SOC under the BBDST working conditions. (c) Correction value based on the UKF algorithm. (d) Error of the SOC under the BBDST working conditions.

Figure 9a shows that both the BP-UKF algorithm and the ABP-UKF algorithm try to approach the reference value, and Figure 9b shows the fluctuation of the ABP-UKF is smaller than that of the BP-UKF algorithm, while the correction value is higher and more accurate, which can partly explain why the proposed algorithm can effectively correct the error estimated by the UKF algorithm; the proposed algorithm has better tracking performance. It can be seen from the correction error curve in Figure 9c that the convergence of the ABP-UKF algorithm is better than the BP-UKF algorithm, and the correction value is stable within a certain error range. Figure 9d shows the maximum error estimated by the UKF algorithm is 4.22%, due to the fluctuation of the estimation of the BP-UKF algorithm; its maximum error reaches 4.57%; the ABP-UKF algorithm optimizes it to a certain extent; the maximum error is 2.93%. Under the BBDST working conditions, the maximum fluctuation values sometimes deviate from the UKF estimates, but the errors of the BP-UKF algorithm can be well corrected under the estimation of the ABP-UKF algorithm, which has a higher estimation accuracy than the UKF algorithm. The criteria for the SOC estimation results under the BBDST working conditions are shown in Table 3.



**Table 3.** Criteria for the SOC estimation results under the BBDST working conditions.

Reference Value	Algorithm	MAX	MAE	RMSE
Ah	UKF	0.04219	0.01957	0.02405
	BP-UKF	0.04571	0.01777	0.02261
	ABP-UKF	0.02959	0.01472	0.01701
UKF	BP <sub>cor</sub>	0.02041	0.00595	0.00736
	ABP <sub>cor</sub>	0.01846	0.01472	0.01375

Combined with Figure 9 and Table 3, the SOC estimation results obtained by the Ah-integral method as the reference value show that the maximum value of the proposed algorithm is the minimum estimation error. The MAE and RMSE are as small as possible, and the ABP-UKF performs best, like under the HPPC working conditions. Combined with the overall error estimation, it can be obtained that the initial value correction effect of the ABP algorithm on the UKF algorithm is greater than that of the BP algorithm, although the correction value of the ABP algorithm is less than the correction value of the BP algorithm, and the BP algorithm had better performance regarding the MAE and RMSE; the effectiveness of the correction performance of the ABP algorithm on the overall compensation is proven.

### 3.3.3. Analysis of the Results under DST Working Conditions

After verification under the BBDST working conditions, the verification results of the international dynamic test conditions needed to be considered. Therefore, the algorithm proposed in this research was further verified by the DST working conditions. The SOC estimation results verified by the DST operating conditions are shown in Figure 10. Figure 10a shows that the inclusion of the BP neural network algorithm as the error correction algorithm has a certain error correction effect, and from Figure 10b, it can be seen that the fluctuation of the ABP-UKF algorithm is smaller than that of the BP-UKF algorithm; the correction value is higher, indicating that the proposed algorithm can effectively correct the error estimated by the UKF algorithm, and the proposed algorithm has better tracking performance, as well; this proves the validity of the corrected error curve in Figure 10c again; although both are stable within a certain compensation value, the former has a smaller amplitude than the latter. Figure 10d shows that the maximum error estimated by the UKF algorithm is 5.03%, the maximum error estimated by the BP-UKF algorithm is 3.37%, and the maximum error of the ABP-UKF algorithm is 2.79%; under the DST working conditions, the BP-UKF algorithm can compensate the estimated value of the UKF to a certain extent, but its estimated smoothness is not as good as the UKF algorithm; however, under the ABP-UKF algorithm, the compensation oscillations of the BP-UKF algorithm can be largely attenuated under the estimation of the ABP-UKF algorithm. Table 4 gives the criteria for the SOC estimation results under the DST working conditions.

Analysing of Figure 10 and Table 4, the estimation result of the BP-UKF algorithm and the ABP-UKF algorithm under the DST working conditions is almost the same; the BP-UKF algorithm performs better under the two standards measures of the MAE and RMSE, while the ABP-UKF algorithm estimates the error value as the minimum value, which demonstrates the purpose of proposing the algorithm. In terms of the superiority of the correction effect, the ABP-UKF algorithm can make the overall value closer to the reference value to an extent, and in the final SOC estimation result, the ABP-UKF algorithm's estimation performance is improved.

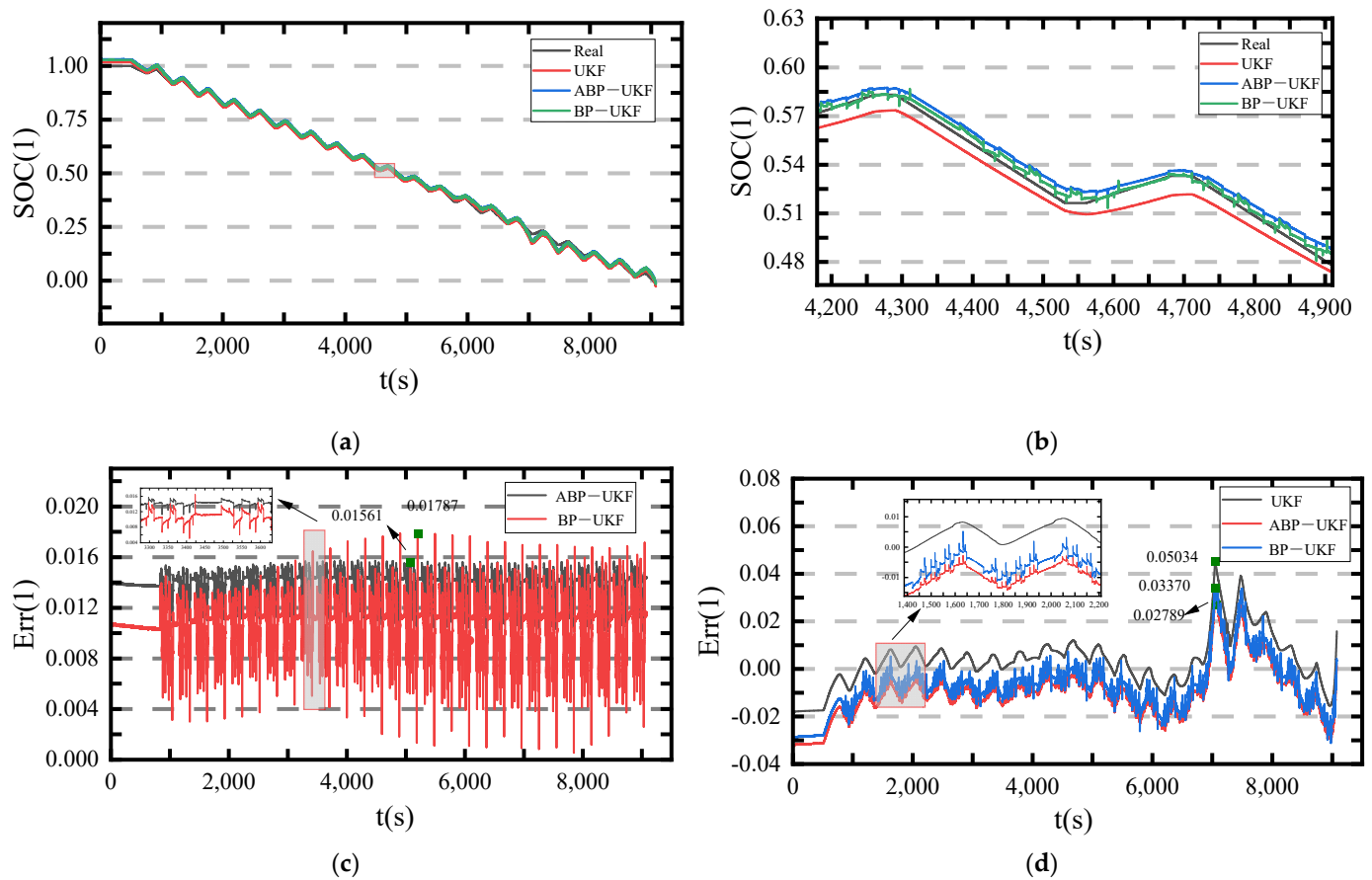


**Figure 10.** SOC estimation and error comparison under DST. (a) Estimation results of the SOC under the DST working conditions. (b) Enlarged view of the estimation results of the SOC under the DST working conditions. (c) Correction value based on the UKF algorithm. (d) Error of the SOC under the DST working conditions.

**Table 4.** Criteria for the SOC estimation results under the DST working conditions.

Reference Value	Algorithm	MAX	MAE	RMSE
Ah	UKF	0.05034	0.00819	0.01132
	BP-UKF	0.03370	0.01065	0.01309
	ABP-UKF	0.02789	0.01320	0.01518
UKF	BP <sub>cor</sub>	0.01787	0.01060	0.01069
	ABP <sub>cor</sub>	0.01561	0.01402	0.01395

#### 4. Conclusions

Accurate SOC estimation of lithium-ion batteries has an important role in their safety control. With the segmented identification and simulation of the SO-PEC modelling method proposed in this research, the model verification accuracy reached 98.915%, proving the proposed method can more accurately characterize the operating characteristics of lithium-ion batteries. Under the experimental verification of the final SOC estimation, through the SOC estimation results under the HPPC, BBDST, and DST working conditions, it was clearly shown that the established ABP-UKF estimation model can well correct the error of the UKF algorithm to estimate the SOC and solve the problem of the UKF algorithm having a large error in the process of estimating the SOC. The estimation accuracy was improved by 1.29% under the HPPC working conditions, 1.28% under the BBDST working conditions, and 2.24% under the DST working conditions. The accuracy of algorithm proposed (ABP-UKF) in this study in the estimation of the SOC was improved. The correction of the estimation

error under the three working conditions reached an average of 1.5%, which verified that the ABP-UKF algorithm has a good SOC estimation result, which makes the estimation result closer to the real SOC value of the lithium-ion battery. This research relied on the estimation accuracy of the UKF algorithm to some extent and can be further optimized to improve the accuracy in subsequent studies, and the growth of the BP neural network will also be the direction of future research.

**Author Contributions:** Conceptualization, Y.W. and C.F.; Writing—Original draft preparation, Y.W.; Writing—review & editing, Y.W., Y.X. and S.W.; Supervision, C.F., S.W. and Y.F.; Formal analysis, Y.F.; Funding acquisition, S.W.; Conceptualization, Y.W. and Y.F.; Methodology, Y.W. and Y.X.; Software, Y.W.; Data curation, Y.W., Y.X. and S.W.; Investigation, C.F. All authors have read and agreed to the published version of the manuscript.

**Funding:** This research was funded by National Natural Science Foundation of China grant number No. 62173281.

**Institutional Review Board Statement:** Not applicable.

**Informed Consent Statement:** Not applicable.

**Data Availability Statement:** The experimental data used in this paper are obtained from my own experiments, and the data used in the final results can be found at <https://www.researchgate.net/project/Basic-data-of-battery44Ah>.

**Conflicts of Interest:** The authors declare no conflict of interest.

## References

1. Goud, J.S.; Kalpana, R.; Singh, B. An Online Method of Estimating State of Health of a Li-Ion Battery. *IEEE Trans. Energy Convers.* **2021**, *36*, 111–119. [[CrossRef](#)]
2. Bi, Y.L.; Choe, S.Y. An adaptive sigma-point Kalman filter with state equality constraints for online state-of-charge estimation of a Li(NiMnCo)O<sub>2</sub>/Carbon battery using a reduced-order electrochemical model. *Appl. Energy* **2020**, *258*, 113925. [[CrossRef](#)]
3. Park, M.; Seo, M.; Song, Y.; Kim, S.W. Capacity Estimation of Li-Ion Batteries Using Constant Current Charging Voltage With Multilayer Perceptron. *IEEE Access* **2020**, *8*, 180762–180772. [[CrossRef](#)]
4. Li, H.; Wang, S.; Islam, M.; Bobobee, E.D.; Zou, C.; Fernandez, C. A novel state of charge estimation method of lithium-ion batteries based on the IWOA-AdaBoost-Elman algorithm. *Int. J. Energy Res.* **2022**, *46*, 5134–5151. [[CrossRef](#)]
5. Vilarinho, I.S.; Lopes, A.L.; Carneiro, J.; Pinto, C.; Labrincha, J.A.; Seabra, M.P. A New Added-Value Application for Steel Wire Drawing Mill Scale Waste in Stoneware Ceramic Products. *Metals* **2021**, *11*, 661. [[CrossRef](#)]
6. Wittkowski, A.; Schirmer, T.; Qiu, H.; Goldmann, D.; Fittschen, U.E.A. Speciation of Manganese in a Synthetic Recycling Slag Relevant for Lithium Recycling from Lithium-Ion Batteries. *Metals* **2021**, *11*, 188. [[CrossRef](#)]
7. Liu, X.; Jin, Y.; Zeng, S.; Chen, X.; Feng, Y.; Liu, S.; Liu, H. Online Identification of Power Battery Parameters for Electric Vehicles Using a Decoupling Multiple Forgetting Factors Recursive Least Squares Method. *CSEE J. Power Energy Syst.* **2020**, *6*, 735–742.
8. Wang, J.; Shen, B.; Wang, Z.; Alsaadi, F.E.; Alharbi, K.H. State-of-charge estimation for Li-ion batteries with uncertain parameters and uncorrelated/correlated noises: A recursive approach. *Int. J. Syst. Sci.* **2021**, *52*, 1675–1691. [[CrossRef](#)]
9. Adaikkappan, M.; Sathiyamoorthy, N. Modeling, state of charge estimation, and charging of lithium-ion battery in electric vehicle: A review. *Int. J. Energy Res.* **2022**, *46*, 2141–2165. [[CrossRef](#)]
10. Mc Carthy, K.; Gullapalli, H.; Ryan, K.M.; Kennedy, T. Review-Use of Impedance Spectroscopy for the Estimation of Li-ion Battery State of Charge, State of Health and Internal Temperature. *J. Electrochem. Soc.* **2021**, *168*, 080517. [[CrossRef](#)]
11. Roselyn, J.P.; Ravi, A.; Devaraj, D.; Venkatesan, R. Optimal SoC Estimation Considering Hysteresis Effect for Effective Battery Management in Shipboard Batteries. *IEEE J. Emerg. Sel. Top. Power Electron.* **2021**, *9*, 5533–5541. [[CrossRef](#)]
12. Chen, Y.; Chen, K.-H.; Sanchez, A.J.; Kazyak, E.; Goel, V.; Gorlin, Y.; Christensen, J.; Thornton, K.; Dasgupta, N.P. Operando video microscopy of Li plating and re-intercalation on graphite anodes during fast charging. *J. Mater. Chem. A* **2021**, *9*, 23522–23536. [[CrossRef](#)]
13. Marchgraber, J.; Gawlik, W.; Wailzer, G. Reducing SoC-Management and losses of battery energy storage systems during provision of frequency containment reserve. *J. Energy Storage* **2020**, *27*, 101107. [[CrossRef](#)]
14. Möller, S.; Satoh, T.; Ishii, Y.; Teßmer, B.; Guerdelli, R.; Kamiya, T.; Fujita, K.; Suzuki, K.; Kato, Y.; Wiemhöfer, H.-D.; et al. Absolute Local Quantification of Li as Function of State-of-Charge in All-Solid-State Li Batteries via 2D MeV Ion-Beam Analysis. *Batteries* **2021**, *7*, 41. [[CrossRef](#)]
15. George, G.A.; Chacko, F.M.; Prince, A.; Jayan, M.V. Integrated fuzzy-based modular cell balancing using mono circuitry for electric vehicle applications. *Electr. Eng.* **2021**, *103*, 153–165. [[CrossRef](#)]
16. Li, L.; Wang, C.; Yan, S.; Zhao, W. A combination state of charge estimation method for ternary polymer lithium battery considering temperature influence. *J. Power Sources* **2021**, *484*, 229204. [[CrossRef](#)]

17. Li, Y.; Vilathgamuwa, D.M.; Farrell, T.W.; Tran, N.T. Selection of equivalent circuit model of Li-ion battery in electrochemical impedance spectroscopy. *Battery Bimon.* **2019**, *49*, 116–120.
18. Jiang, H.; Zhang, W.; Chen, L.; Li, H. Electrochemical modeling of Li-ion battery based on electrical double layer structure. *Battery Bimon.* **2018**, *48*, 244–248.
19. Xie, H.; Han, B.; Song, H.; Li, X.; Kang, Y.; Zhang, Q. In-situ measurements of electrochemical stress/strain fields and stress analysis during an electrochemical process. *J. Mech. Phys. Solids* **2021**, *156*, 104602. [[CrossRef](#)]
20. Song, W.; Chen, M.; Bai, F.; Feng, Z. Thermal performance and optimization of Li-ion battery based on thermal-electro coupled model. *Battery Bimon.* **2018**, *48*, 309–312.
21. Duan, X.; Jiang, W.; Zou, Y.; Lei, W.; Ma, Z. A coupled electrochemical-thermal-mechanical model for spiral-wound Li-ion batteries. *J. Mater. Sci.* **2018**, *53*, 10987–11001. [[CrossRef](#)]
22. Vu, H.; Shin, W.D. Scheduled Pre-Heating of Li-Ion Battery Packs for Balanced Temperature and State-of-Charge Distribution. *Energies* **2020**, *13*, 2212. [[CrossRef](#)]
23. Xu, W.; Wang, S.; Jiang, C.; Fernandez, C.; Yu, C.; Fan, Y.; Cao, W. A novel adaptive dual extended Kalman filtering algorithm for the Li-ion battery state of charge and state of health co-estimation. *Int. J. Energy Res.* **2021**, *45*, 14592–14602. [[CrossRef](#)]
24. How, D.N.T.; Hannan, M.A.; Lipu, M.S.H.; Sahari, K.S.M.; Ker, P.J.; Muttaqi, K.M. State-of-Charge Estimation of Li-Ion Battery in Electric Vehicles: A Deep Neural Network Approach. *IEEE Trans. Ind. Appl.* **2020**, *56*, 5565–5574. [[CrossRef](#)]
25. Ming, T.T.; Zhao, J.; Wang, X.L.; Wang, K. SOC estimation of a lithium battery under high pulse rate condition based on improved LSTM. *Power Syst. Prot. Control.* **2021**, *49*, 144–150.
26. Lin, X.; Wu, J.; Wei, Y. An ensemble learning velocity prediction-based energy management strategy for a plug-in hybrid electric vehicle considering driving pattern adaptive reference SOC. *Energy* **2021**, *234*, 121308. [[CrossRef](#)]
27. Nath, A.; Gupta, R.; Mehta, R.; Bahga, S.S.; Gupta, A.; Bhasin, S. Attractive Ellipsoid Sliding Mode Observer Design for State of Charge Estimation of Lithium-Ion Cells. *IEEE Trans. Veh. Technol.* **2020**, *69*, 14701–14712. [[CrossRef](#)]
28. Liu, X.; Li, K.; Wu, J.; He, Y.; Liu, X. State of Charge Estimation for Traction Battery Based on EKF-SVM Algorithm. *Automot. Eng.* **2020**, *42*, 1522–1528, 1544.
29. Qaisar, S.M. A Proficient Li-Ion Battery State of Charge Estimation Based on Event-Driven Processing. *J. Electr. Eng. Technol.* **2020**, *15*, 1871–1877. [[CrossRef](#)]
30. Sun, Y.; Jiang, Z. Simulation of thermal runaway diffusion in overcharging of Li-ion battery module. *Battery Bimon.* **2019**, *49*, 481–484.
31. Babaeiyazdi, I.; Rezaei-Zare, A.; Shokrzadeh, S. State of charge prediction of EV Li-ion batteries using EIS: A machine learning approach. *Energy* **2021**, *223*, 120116. [[CrossRef](#)]
32. Jiao, M.; Wang, D.; Yang, Y.; Liu, F. More intelligent and robust estimation of battery state-of-charge with an improved regularized extreme learning machine. *Eng. Appl. Artif. Intell.* **2021**, *104*, 104407. [[CrossRef](#)]
33. Lotfi, F.; Ziapour, S.; Faraji, F.; Taghirad, H.D. A switched SDRE filter for state of charge estimation of lithium-ion batteries. *Int. J. Electr. Power Energy Syst.* **2020**, *117*, 105666. [[CrossRef](#)]
34. Tsukada, M.; Kondo, M.; Matsutani, H. A Neural Network-Based On-Device Learning Anomaly Detector for Edge Devices. *IEEE Trans. Comput.* **2020**, *69*, 1027–1044. [[CrossRef](#)]
35. El-Sehiemy, R.A.; Hamida, M.A.; Mesbahi, T. Parameter identification and state-of-charge estimation for lithium-polymer battery cells using enhanced sunflower optimization algorithm. *Int. J. Hydrog. Energy* **2020**, *45*, 8833–8842. [[CrossRef](#)]
36. Jiang, H.; Chen, X.; Liu, Y.; Zhao, Q.; Li, H.; Chen, B. Online State-of-Charge Estimation Based on the Gas-Liquid Dynamics Model for Li(NiMnCo)O<sub>2</sub> Battery. *Energies* **2021**, *14*, 324. [[CrossRef](#)]
37. Parhizi, M.; Pathak, M.; Jain, A. Analytical Model Based Prediction of State-of-Charge (SoC) of a Lithium-Ion Cell under Time-Varying Charge/Discharge Currents. *J. Electrochem. Soc.* **2020**, *167*, 120544. [[CrossRef](#)]
38. Malkhandi, A.; Senroy, N.; Mishra, S. A Dynamic Model of Impedance for Online Thevenin's Equivalent Estimation. *IEEE Trans. Circuits Syst. II-Express Briefs* **2022**, *69*, 194–198. [[CrossRef](#)]
39. Guo, D.; Yang, G.; Han, X.; Feng, X.; Lu, L.; Ouyang, M. Parameter identification of fractional-order model with transfer learning for aging lithium-ion batteries. *Int. J. Energy Res.* **2021**, *45*, 12825–12837. [[CrossRef](#)]
40. Ren, P.; Wang, S.; He, M.; Cao, W. Novel strategy based on improved Kalman filter algorithm for state of health evaluation of hybrid electric vehicles Li-ion batteries during short- and longer term operating conditions. *J. Power Electron.* **2021**, *21*, 1190–1199. [[CrossRef](#)]